Supporting Online Material for

Crystal Structure of the Human K2P TRAAK, a Lipid- and Mechano-Sensitive K^+ Ion Channel

Stephen G. Brohawn[1], Josefina del Mármol[1], Roderick MacKinnon[1]

[1]Laboratory of Molecular Neurobiology and Biophysics, The Rockefeller University, Howard Hughes Medical Institute, 1230 York Avenue, New York, New York 10065, USA.

correspondence to: Roderick.MacKinnon@rockefeller.edu

This PDF file includes:

Materials and Methods

Cloning, expression, and purification. A gene corresponding to *H. sapiens* TRAAK (GI:13124080) amino acids 1-419 was codon-optimized for eukaryotic expression, synthesized (Genewiz, Inc.), amplified by PCR, and ligated into the EcoR1/Xho1 restriction sites of a modified pPICZ-B vector (Invitrogen). The resulting protein is linked at the C-terminus to EGFP and a 10xHis tag via a short linker (SNS) followed by a PreScission protease cleavage site (LEVLFQ/GP). Purified full-length protein did not crystallize and was N-glycosylated (data not shown). The construct was modified by PCR to truncate the C-terminal 119 residues and mutate two predicted N-linked glycosylation sites (N104Q, N108Q) for crystallization. Human $TRAAK_{1-300(N104Q,N108Q)}$-SNS-LEVLFQ/GP-EGFP-H10 is referred to as TRAAK in the text for clarity.

Vector was linearized with Pme1 and transformed into *P. pastoris* strain SMD1163 by electroporation. Transformants were selected by plating on YPDS plates with 1mg/mL zeocin. Expression levels of individual clones were compared by FSEC screening of small-scale culture inductions (*43*). Large-scale expression was performed in a fermentor. Overnight cultures of cells grown in YPD with 1mg/mL zeocin were added to 3L minimal media to an OD_{600} ~1 and grown overnight at 29°C with glycerol feeding and pH maintained at 5.0 by addition of NH_4OH. Cells were then starved to deplete glycerol, temperature was reduced to 27°C, and induction was initiated with slow addition of methanol. Expression continued for ~48-60 hours. Cells were pelleted, frozen in liquid nitrogen, and stored at -80°C.

Cells were disrupted by milling (Retsch model MM301) 5 times for 3 minutes at 25 Hz. All subsequent purification steps were carried out at 4° C. Cell powder was added to lysis buffer (50 mM Tris pH 8.0, 150 mM KCl, 60 mM dodecyl-β-D-maltoside (DDM, Affymetrix), 0.1 mg/mL DNAse 1, 0.1 μg/ml pepstatin, 1 μg/ml leupeptin, 1 μg/ml aprotinin, 0.1 mg/ml soy trypsin inhibitor, 1 mM benzamidine, and 0.1 mg/ml AEBSF, with 1 mM phenylmethysulfonyl fluoride added immediately before use) at a ratio of 1g cell pellet/4mL lysis buffer. Membranes were extracted for 3 hours with gentle stirring followed by centrifugation at 35000xg for 45 minutes. Cobalt resin (Clontech) was added to the supernatant (1mL resin / 5g cell pellet) and stirred gently for 3 hours. Resin was collected on a column and serially washed and eluted in IMAC buffer (50 mM Tris pH 8.0, 150 mM KCl, 6 mM DDM) with 10 mM, 30 mM, and 300 mM imidazole pH 8.0. EDTA (1mM final) and PreScission protease (~1:50 wt:wt) were added to the elution before incubation with gentle rocking overnight. Cleaved protein was concentrated and applied to a Superdex 200 column (GE Healthcare) equilibrated in SEC buffer (20 mM Tris pH 8.0, 150 mM KCl, 1 mM EDTA, 1 mM DDM). For Tl^+ bound crystals, protein was prepared identically except for substitution of KNO_3 for KCl in lysis and IMAC buffers and $TlNO_3$ for KCl in SEC buffer.

Crystallization and structure determination. Pure protein was concentrated (50kDa MWCO, Millipore) to ~ 10 mg/mL for crystallization. 0.4 μL protein was added to 0.9 μL reservoir (21-24% PEG400) in hanging drops. The largest crystals appeared within 1 week and grew to full size cuboids with two approximately equal length faces (~ 0.15 x 0.15 x 0.4 mm) in 3-6 weeks at 4° C. Crystals were cryoprotected by addition of 1 μL SEC buffer with 30% PEG400 to drops and immediately harvested and frozen in

liquid nitrogen. CH_3Hg^+-derivatived crystals were prepared by adding a trace amount of solid CH_3HgCl to drops with crystals and incubating over reservoir for 4-12 hours before harvesting. Crystal mother liquor and cryoprotection solution was supplemented with 1 mM n-dodecylphosphocholine (Fos-choline-12, Affymetrix) for native and CH_3Hg^+-derivative crystals as it was found to improve x-ray diffraction.

Data were collected for native and Tl^+ crystals at APS beamline 23-IDD and for CH_3Hg^+-derivatized crystals at APS beamline 23-IDB and processed with HKL2000 (*44*). Data were anisotropic and native data were elliptically truncated and scaled (*45*) to 3.8 x 3.3 x 3.8 Å prior to anisotropic scaling with Phaser (*46*) and sharpening by application of a negative isotropic B factor of -74 to the data.

Seven Tl^+ sites were located by Shelx (*47*) and refined with Sharp (*48*) from the Tl^+ derivative data in a multiple-wavelength with anomalous dispersion (MAD) experiment. Positions and phases were further refined in Sharp using isomorphous and anomalous differences in a MAD plus native experimental configuration. Density modification resulted in continuous and interpretable electron density for the majority of the channel (fig. S5). There are two TRAAK protomers forming one channel in the asymmetric unit. Utilization of an early stage helical model during initial rounds of density modification in Sharp to guide solvent envelope estimation improved definition of fine features and weakly defined loop regions in the experimental map. For register information, cysteines in native crystals were derivatized with CH_3Hg^+. Five Hg sites were consistently found with PhaserEP (*49*) in multiple datasets from derivatized crystals using partially refined models of TRAAK as starting phase information. Use of PhaserEP to search log-likelihood gradient maps was found to be more sensitive than searching

model-phased anomalous difference Fourier maps for the weaker Hg sites. The Hg positions correspond to 5 of the 8 cysteines in the asymmetric unit: C146 and C206 from each protomer and C218 in protomer B. One cysteine from each protomer is disulfide bonded at the top of the helical cap and so is not expected to react with CH_3Hg^+. C218 in protomer A is either not observed crystallographically as a Hg^+ adduct due to disorder or is not chemically modified.

The channel was modeled by iterative manual building in Coot (*50*) and refinement in Refmac (*51*). A late stage model was improved by refinement in CNS with simulated annealing and a deformable elastic network using the starting model as a reference structure (*52*). Refinement was aided by incorporation of experimental phase and two-fold local NCS restraints and converged to an R_{free}=32.3% with good geometry (Table S1). Strict two-fold NCS restraints were not used, as there exist small but significant differences in the relative orientations of some regions of the channel including the outer helices and helical cap. Two loops and residues at each protomer terminus were not modeled due to lack of interpretable electron density. The final model consists of TRAAK residues 25-106, 112-187, and 190-290 in protomer A, residues 27-104, 112-179, and 193-290 in protomer B, and five K^+ ions.

We note that while protein mediated crystal contacts between the helical cap and the pore domain 1-2 linking region are observed along the **b** axis in the crystal, both **a** and **c** axes lack well defined protein mediated contacts (Fig. S6). While consistent with the severe anisotropy of the data (strong **b** direction, weak **a** and **c** directions), poor packing can be indicative of incorrect space group determination as a result of apparent pseudosymmetry. Molecular replacement in each of the other seven primitive

orthorhombic enantiomorphs followed by refinement of the top solutions failed to produce a convincing solution with observable packing in all lattice directions. Attempts to find solutions in alternatively processed data (in primitive monoclinic, centered monoclinic, centered orthorhombic, and primitive tetragonal lattices) also failed. There are 24 residues at the N terminus and 19 (10 from TRAAK and 9 remaining from the linker and protease cleavage site) at the C terminus of each protomer that are unmodeled due to poor electron density. Either of these regions if even partly extended would be of sufficient length to bridge the ~20Å gap between channel layers in the crystal. Alternatively, detergent molecules/micelles or other solvent molecules may contribute to lattice formation. Regardless, we are confident that our ability to refine the structure to good statistics indicates a reliable model.

Electrophysiological recordings from CHO cells. Full length TRAAK and the truncated and mutated TRAAK construct used for crystallization were cloned into a pCEH vector for mammalian cell expression. CHO cells (ATCC) were maintained in DMEM-F12 (Gibco) containing 10% FBS. Cells were plated onto poly-D-lysine-coated glass coverslips (BD BioCoat) ~24 hrs before transfection with Lipofectamine2000 (Invitrogen) following manufacturers protocol. After 48-72 hrs, coverslips were transferred to the recording chamber. Immediately before recording, media was replaced by bath solution. All recordings were performed at room temperature. Recordings were obtained with an Axopatch 200B amplifier (Molecular Devices) using standard whole-cell patch-clamp and excised outside-out patch techniques. Recordings were filtered at 1 kHz with sampling at 10 kHz. Pipettes of 1.5-2 MΩ resistance (for whole cell recordings) and 2-3 MΩ resistance (for outside-out patch recordings) were pulled from borosilicate

glass and fire polished. Currents were recorded during voltage steps from -100 to 40 mV in 10mV increments from a holding potential of -80 mV. Voltage ramps were obtained by holding at -100mV and increasing to 40mV in 800 msec. For arachidonic acid (AA) activation experiments, cells were continuously perfused with either bath solution or bath solution containing 100 μM AA. Currents were recorded from the same cell before and ~1 min after perfusion of AA. For pressure activation experiments, positive pressure was applied to patches through a syringe connected to the pipette. Pipette solution was 150 mM KCl, 3 mM $MgCl_2$, 5 mM EGTA, 10 mM Hepes (pH 7.2). Bath solution was 3 mM $MgCl_2$, 1 mM $CaCl_2$, 10 mM Hepes (pH 7.3) and 15 mM KCl and 135 mM NaCl for activation experiments and either 5 mM KCl and 145 mM NaCl, 15 mM KCl and 135 mM NaCl, 70 mM KCl and 80 mM NaCl or 150 mM KCl for voltage ramp experiments.

Reconstitution in lipid vesicles. Purification of TRAAK was carried out identically except SEC buffer was 20 mM Hepes pH 8.0, 150 mM KCl, 1 mM EDTA, 1 mM DDM. Protein was concentrated to 1 mg/mL and added to 10mg/mL 1-palmitoyl-2-oleoyl-*sn*-glycero-3-phosphoethanolamine: 1-palmitoyl-2-oleoyl-*sn*-glycero-3-phospho-(1'-rac-glycerol) (POPE:POPG) (3:1) lipid vesicles in dialysis buffer (20mM Hepes pH 7.4, 150 mM KCl, 1 mM EDTA) with 10 mM DDM at a protein to lipid ratio of 1:100 (w/w). The mixture was rocked overnight before dialyzing in 50 kDa MWCO tubing for 1 week against 10 4L changes of dialysis buffer with Bio-Beads (Bio-Rad) added to the final three changes. Vesicles were frozen in liquid nitrogen and aliquots stored at -80°C until required.

Flux assay. Frozen vesicles were thawed and briefly sonicated prior to the assay. 10 μL of vesicles were added to 190 μL of flux assay buffer (20 mM Hepes pH 7.4, 150

mM NaCl, 1 mM EDTA, 2 μM 9-amino-6-chloro-2-methoxyacridine (ACMA)). Fluorescence was recorded every 10 seconds (excitation λ=410nm, emission λ=490nm). After 30 seconds of baseline fluorescence was monitored, K^+ flux was initiated by addition of 1 μM *m*-chlorophenyl hydrazone (CCCP) to collapse the electrical potential. The chemical gradient was terminated by addition of the K^+ ionophore valinomycin to 0.02 μM and fluorescence was monitored until equilibrium reached.

Lipid bilayer recordings. Vesicles from the same reconstitution used for the flux assay were thawed and briefly sonicated prior to use. Bilayer experiments were performed essentially as previously described (*53*). Planar lipid bilayers of 3:1 (w:w) 1,2-diphytanoyl-*sn*-glycero-3-phosphocholine:1-palmitoyl-2-oleoyl-*sn*-glycero-3-phosphate (DPhPc:POPA) were painted over a 300 μM polystyrene hole separating two chambers. Vesicles were added to the *cis* chamber filled with 4 mL 10 mM Hepes pH 7.5, 150 mM KCl while the *trans* side contained 3 mL 10 mM Hepes pH 7.5, 15 mM NaCl. Once vesicles were fused with the bilayer NaCl was made 150 mM on the *trans* side. Measurements were made with the voltage-clamp method in whole-cell mode using an Axopatch 200B amplifier, a DigiData 1440A analogue-to- digital converter, and Clampex software (Axon instruments). Analogue data were filtered at 1 kHz and sampled at 10 kHz.

Software. Crystallographic programs from the CCP4 suite were used throughout structure determination (*54*). Structure figures were generated with Pymol (*55*). Alignments were made with MAFFT (*56*) and visualized with JalView (*57*).

A

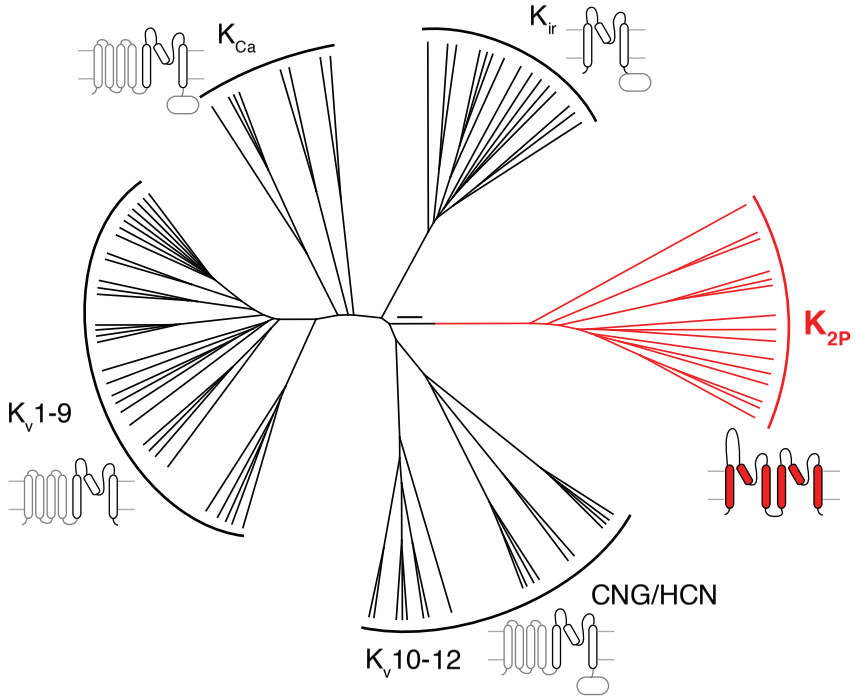

B

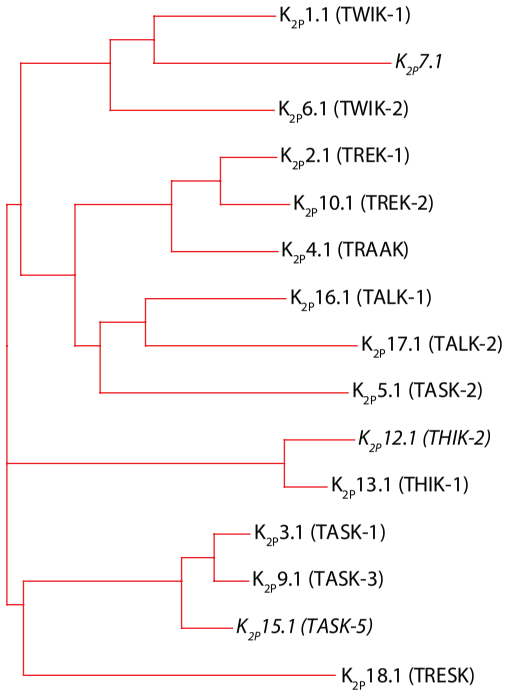

C

	TRAAK (K2P_4.1)													
TREK1 (K2P_2.1)	39.2	TREK1 (K2P_2.1)												
TREK2 (K2P_10.1)	41.0	59.0	TREK2 (K2P_10.1)											
TWIK1 (K2P_1.1)	28.0	29.7	29.6	TWIK1 (K2P_1.1)										
TWIK2 (K2P_6.1)	33.0	29.3	28.1	44.3	TWIK2 (K2P_6.1)									
TWIK3 (K2P_7.1)	28.2	25.4	28.4	39.3	33.2	TWIK3 (K2P_7.1)								
TALK1 (K2P_16.1)	33.2	30.1	30.2	28.1	30.4	28.5	TALK1 (K2P_16.1)							
TALK2 (K2P_17.1)	35.0	30.5	27.5	24.3	31.0	25.1	35.2	TALK2 (K2P_17.1)						
TASK2 (K2P_5.1)	28.0	27.3	25.9	27.0	28.4	23.5	30.9	31.4	TASK2 (K2P_5.1)					
THIK2 (K2P_12.1)	24.9	25.7	23.5	25.9	27.0	25.8	26.3	23.1	24.9	THIK2 (K2P_12.1)				
THIK1 (K2P_13.1)	25.5	23.9	23.3	25.8	24.0	22.3	24.7	24.1	23.4	63.8	THIK1 (K2P_13.1)			
TASK1 (K2P_3.1)	27.1	26.3	24.5	29.6	30.2	26.1	29.8	28.3	26.5	24.2	28.2	TASK1 (K2P_3.1)		
TASK3 (K2P_9.1)	23.7	26.2	26.2	27.2	27.9	22.6	28.0	24.4	24.6	21.4	24.1	58.9	TASK3 (K2P_9.1)	
TASK5 (K2P_15.1)	27.8	29.4	27.0	28.5	29.7	27.8	29.2	27.8	29.5	27.4	27.1	51.4	55.1	TASK5 (K2P_15.1)
TRESK (K2P_18.1)	21.9	19.7	20.3	22.1	20.2	20.1	24.9	20.9	20.5	21.1	21.0	23.1	24.4	22.5

Fig. S1.
Evolutionary relationships and unique structural architecture of K2P channels. (A) Unrooted phylogenetic tree of the K^+ ion channel superfamily. The tree was calculated from a sequence alignment of the 88 human K^+ channel superfamily pore domains (*58*). K2P channels form a clade distinct from other K^+ channels (the voltage-gated (K_V1-9), Ca^{2+}-acitivated (K_{Ca}), inward-rectifying (K_{ir}), and cyclic nucleotide-gated (CNG/HCN and K_V10-12 channels)). The architecture of each family is illustrated as a cartoon from N- (left) to C-terminus (right). Note that some K_{Ca} channels contain an S_0 helix placing the N-terminus on the extracellular side. Cylinders represent helices drawn with respect to the membrane (gray lines) with extracellular solution above. A K^+ channel pore domain (black outlines) consists of two membrane spanning helices (the outer and inner helices) flanking a membrane reentrant pore helix and selectivity filter. K2P channels (red) have two concatenated pore domains per protomer, while other channels have one. Accessory domains in other channels are drawn in light gray. **(B)** K2P phylogenetic tree. The tree was calculated from a sequence alignment of the 15 human channel pore domain 1 sequences. The K2P channels can be divided into six subfamilies based on sequence similarity: TRAAK/TREK (TRAAK, TREK-1, and TREK-2), TWIK (TWIK-1 and TWIK-2), TALK (TALK-2 and TASK-2), THIK (THIK-1 and THIK-2), TASK (TASK-1, TASK-3, and TASK-5) and TRESK. Channels for which functional expression has not been demonstrated are italicized in **(B)**. **(C)** Pairwise percentage of identical residues between human K2P channels. Sequence conservation between subfamilies of K2P channels (~20-30%) is comparable to that between channels from other K^+ channel clades (e.g. between K_v and K_{ir} channels).

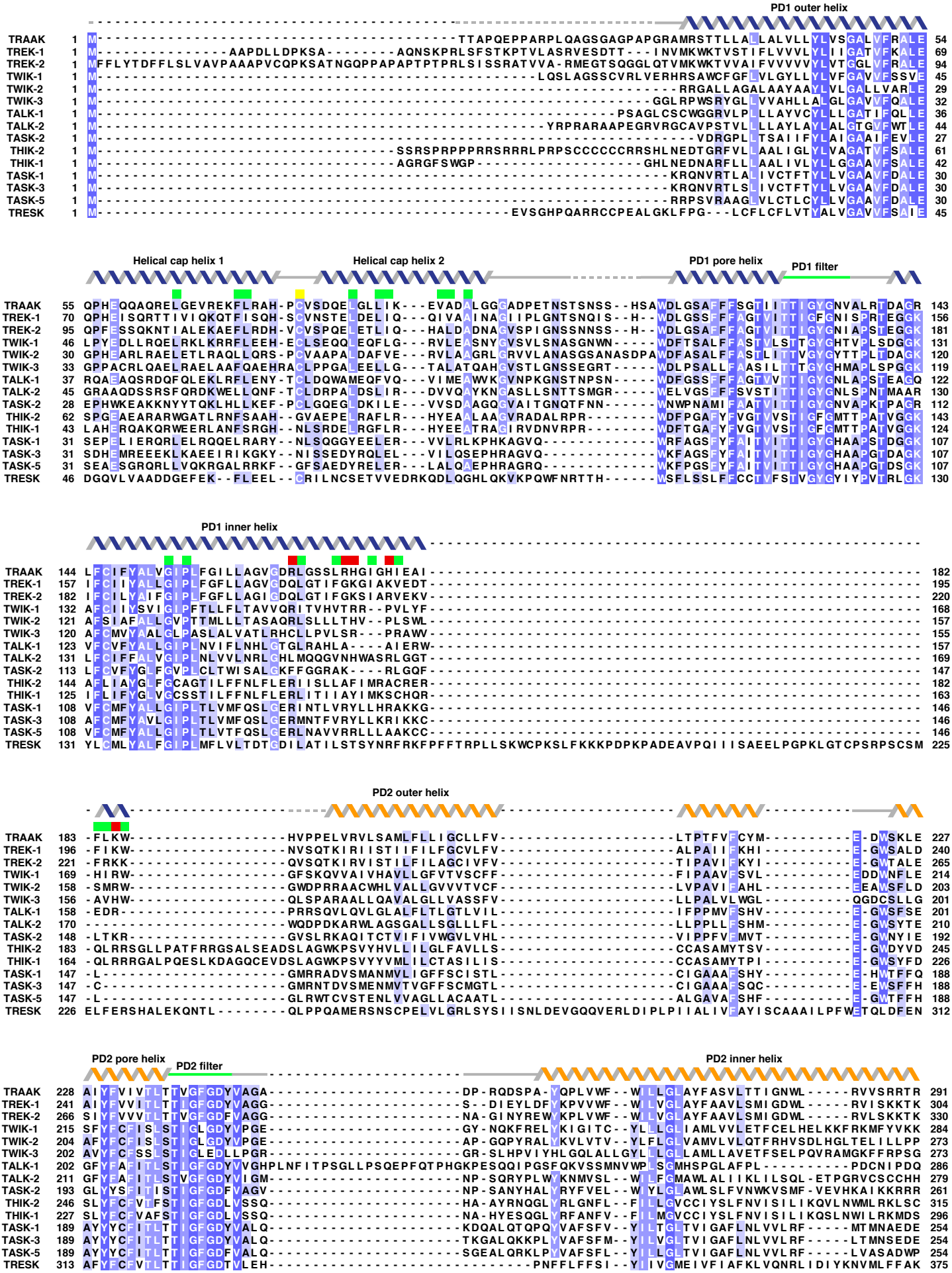
PD1 outer helix
Helical cap helix 1
Helical cap helix 2
PD1 pore helix
PD1 filter
PD1 inner helix
PD2 outer helix
PD2 pore helix
PD2 filter
PD2 inner helix

Fig. S2.

Multiple sequence alignment of human K2P channels. Alignment of the 15 human K2P channels is colored by conservation in a ramp from white (not conserved) to dark blue (highly conserved). Secondary structure of TRAAK is indicated above the sequences and labeled with PD1 and PD2 signifying pore domain 1 and 2, respectively. Large gaps in the alignment are shown as dashed black lines, residues not observed in the crystal structure as dashed gray lines, loops and non-helical secondary structure as solid gray lines, K^+ selectivity filters as green lines, and helices as cartoons. Helices in pore domain 1 are colored blue and helices in pore domain 2 are colored orange. In the helical cap, hydrophobic core-forming residues are marked with green boxes and the disulfide bonded C78 is marked with a yellow box above the sequence. In the amphipathic segment of the pore domain 1 inner helix, hydrophobic residues highlighted in Fig. 5 are marked with green boxes and basic residues highlighted in Fig. 5 are marked with red boxes above the sequence. The hinge glycine (G153) and kink proline (P155) in the pore domain 1 inner helix are also marked with a green box above the sequence. Secondary structure is drawn until the last residue present in the crystal construct of the TRAAK channel (Q300).


PD1 outer helix
Helical cap helix 1
Helical cap helix 2
PD1 pore helix
PD1 filter
PD1 inner helix
PD2 outer helix
PD2 pore helix
PD2 filter
PD2 inner helix
Hs_TRAAK
Rn_TRAAK
Bt_TRAAK
Tn_TRAAK
Hs_TREK1
Gg_TREK1
Dr_TREK1
Tn_TREK1
Hs_TREK2
Gg_TREK2
Xl_TREK2
Dr_TREK2

Fig. S3.

Multiple sequence alignment of TRAAK/TREK K2P channels. Alignment of four TRAAK, four TREK-1, and four TREK-2 channels is colored by conservation in a ramp from white (not conserved) to dark blue (highly conserved). Secondary structure of TRAAK is indicated above the sequences and labeled with PD1 and PD2 signifying pore domain 1 and 2, respectively. Large gaps in the alignment are shown as dashed black lines, residues not observed in the crystal structure as dashed gray lines, loops and non-helical secondary structure as solid gray lines, K^+ selectivity filters as green lines, and helices as cartoons. Helices in pore domain 1 are colored blue and helices in pore domain 2 are colored orange. In the helical cap, hydrophobic core-forming residues are marked with green boxes and the disulfide bonded C78 is marked with a yellow box above the sequence. In the amphipathic segment of the pore domain 1 inner helix, hydrophobic residues highlighted in Fig. 5 are marked with green boxes and basic residues highlighted in Fig. 5 are marked with red boxes above the sequence. The hinge glycine (G153) and kink proline (P155) in the pore domain 1 inner helix are also marked with a green box above the sequence. Secondary structure is drawn until the last residue present in the crystal construct of the TRAAK channel (Q300). Abbreviations used are: Hs, *Homo sapiens*, Rn, *Rattus norvegicus*, Bt, *Bos taurus*, Tn, *Tetraodon nigroviridis*, Gg, *Gallus gallus*, Dr, *Danio rerio*, Xl, *Xenopus laevis*.

A

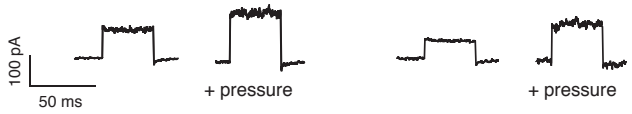
Crystal construct
Full-length
100 pA
50 ms
+ pressure
+ pressure

B

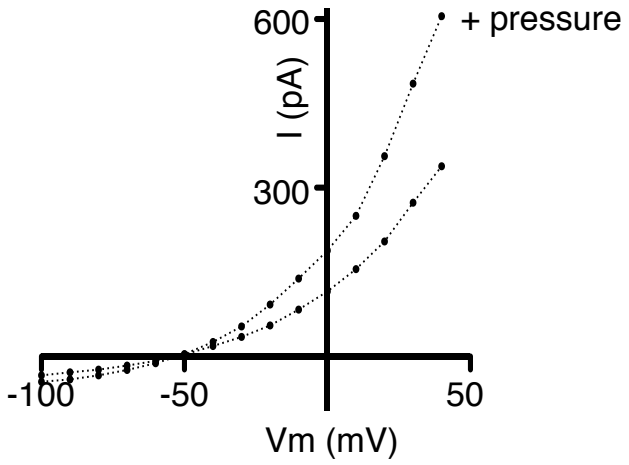
600
300
I (pA)
+ pressure
-100
-50
50
Vm (mV)

Fig. S4.

Pressure activation of TRAAK. (A) Pressure activation of the crystal construct and full-length TRAAK channels. A representative current recording during a voltage pulse from -80 to -10 mV was made before and during the application of positive pressure. **(B)** Current-voltage relationship is plotted from outside-out patch recordings of the crystal construct of the TRAAK channel during voltage pulses from -100 to 40 mV from a holding potential of -80 mV before and during the application of positive pressure through the patch pipette (+ pressure).

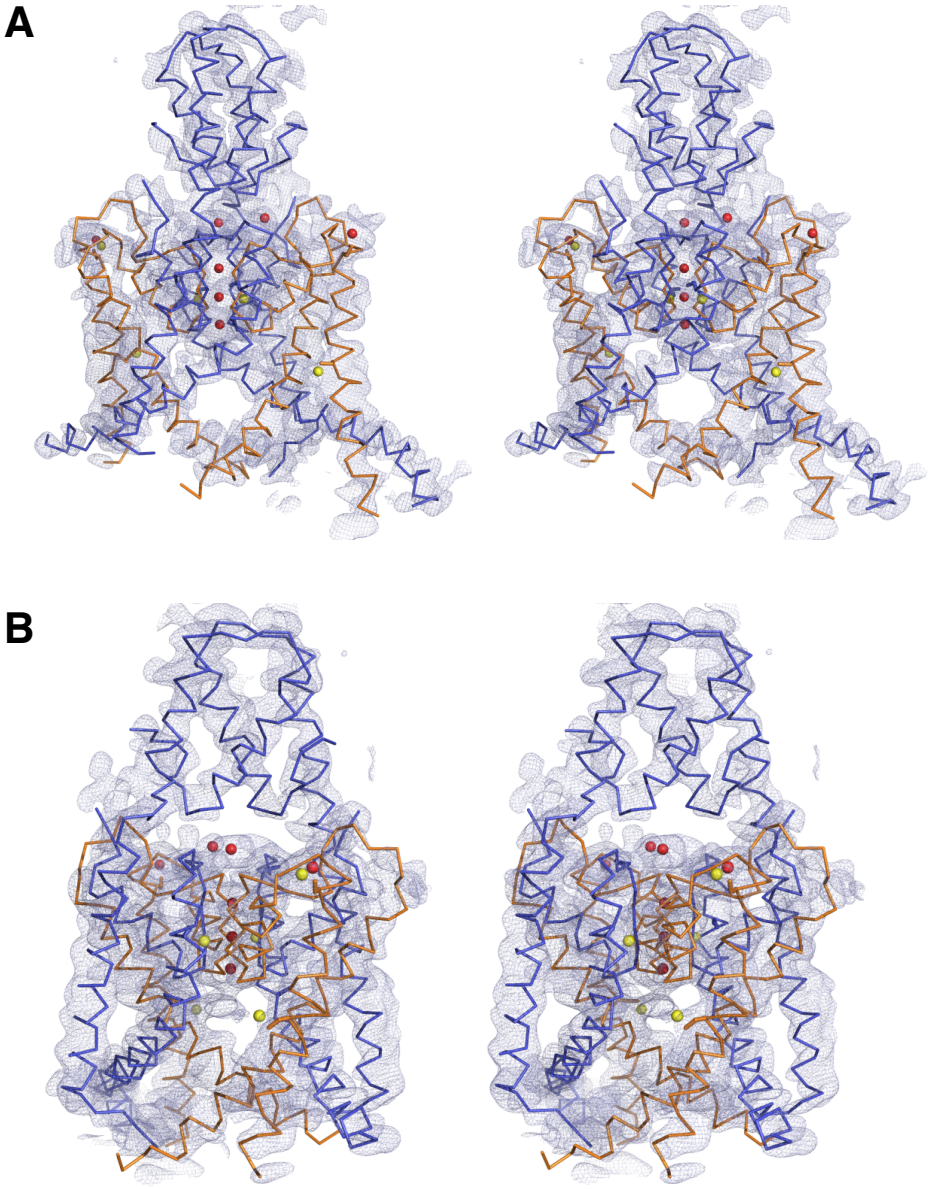
A
B

Fig. S5.

The TRAAK structure solution. (A) Stereo view of TRAAK similar to the view in Fig. 1C. The view in **(B)** is rotated ~70˚ counterclockwise. Electron density (light blue mesh) calculated from experimental phases and used for initial model building is shown around the final TRAAK model in wire representation with pore domain 1 colored blue and pore domain 2 colored orange. Phases were calculated with Sharp (*48*) from a multiple-wavelength isomorphous replacement with anomalous scattering experiment using two-wavelength data from a Tl^+-containing derivative and K^+-containing native data. A solvent fraction of 0.75 was used for density modification within Sharp, the map is calculated from 31-3.3 Å, and is contoured at 1.5σ. Seven Tl^+ sites determined with Sharp are shown as red spheres. Five Hg sites determined from CH_3Hg^+-derivatized crystals with Phaser EP (*49*) using a preliminary TRAAK model as starting phase information are shown as yellow spheres. Cysteine residues in the final TRAAK model proximal to the Hg^+ positions are shown as sticks.

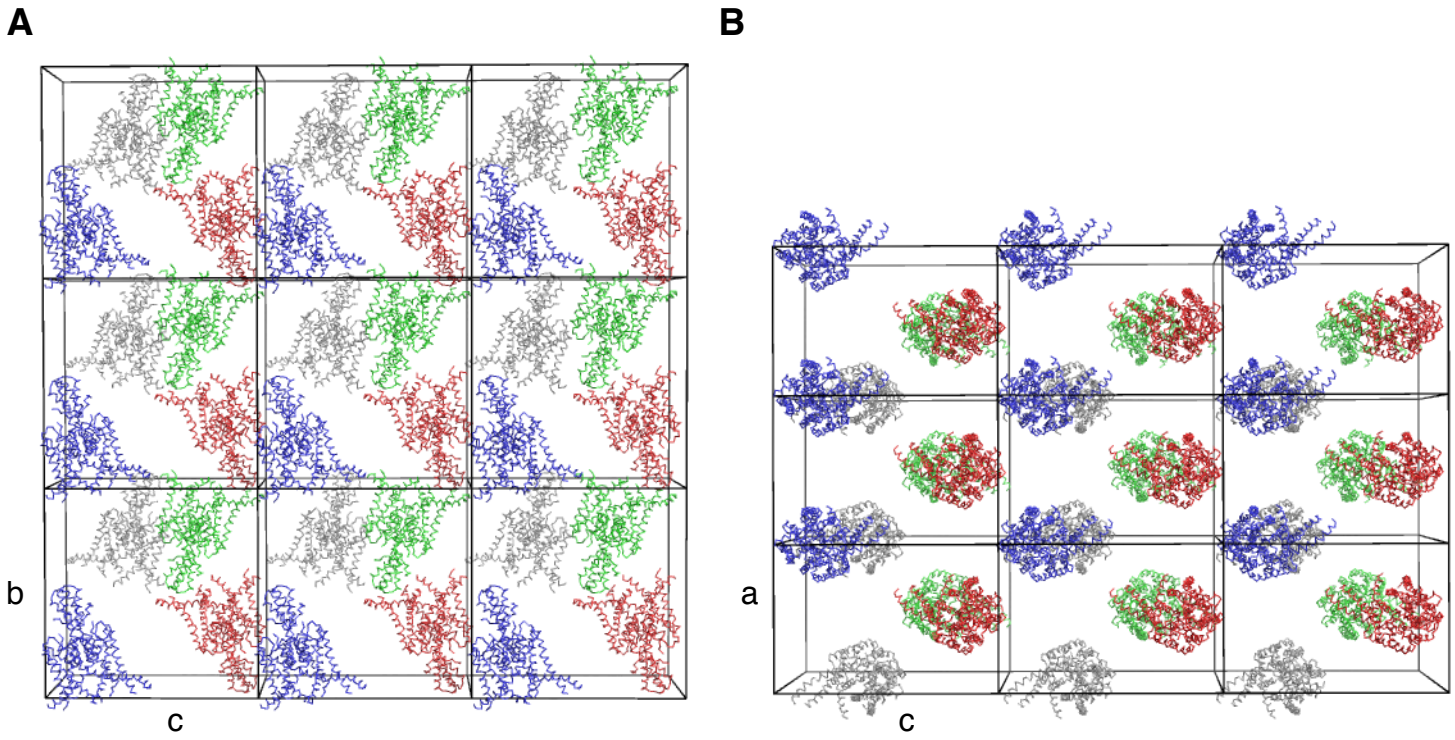
A
B
b
c
a
c

Fig. S6.

TRAAK crystal packing. (A,B) Two views of the TRAAK crystal lattice: along the **a** axis in **(A)** and along the **b** axis in **(B).** Unit cells are drawn as boxes and TRAAK molecules in each unit cell are shown in different color ribbons. Crystals diffracted anisotropically with a strong (3.3 Å) **b** direction and weak (3.8 Å) **a,c** directions. Consistently, well-defined packing interactions exist along the **b** axis, with the helical cap from one channel forming crystal contacts with the cytoplasmic side of the neighboring channel. The **a** and **c** directions, however, lack clear protein-mediated contacts. Presumably micelle- or detergent- mediated contacts and/or poorly discernable protein contacts propagate the lattice in these directions.

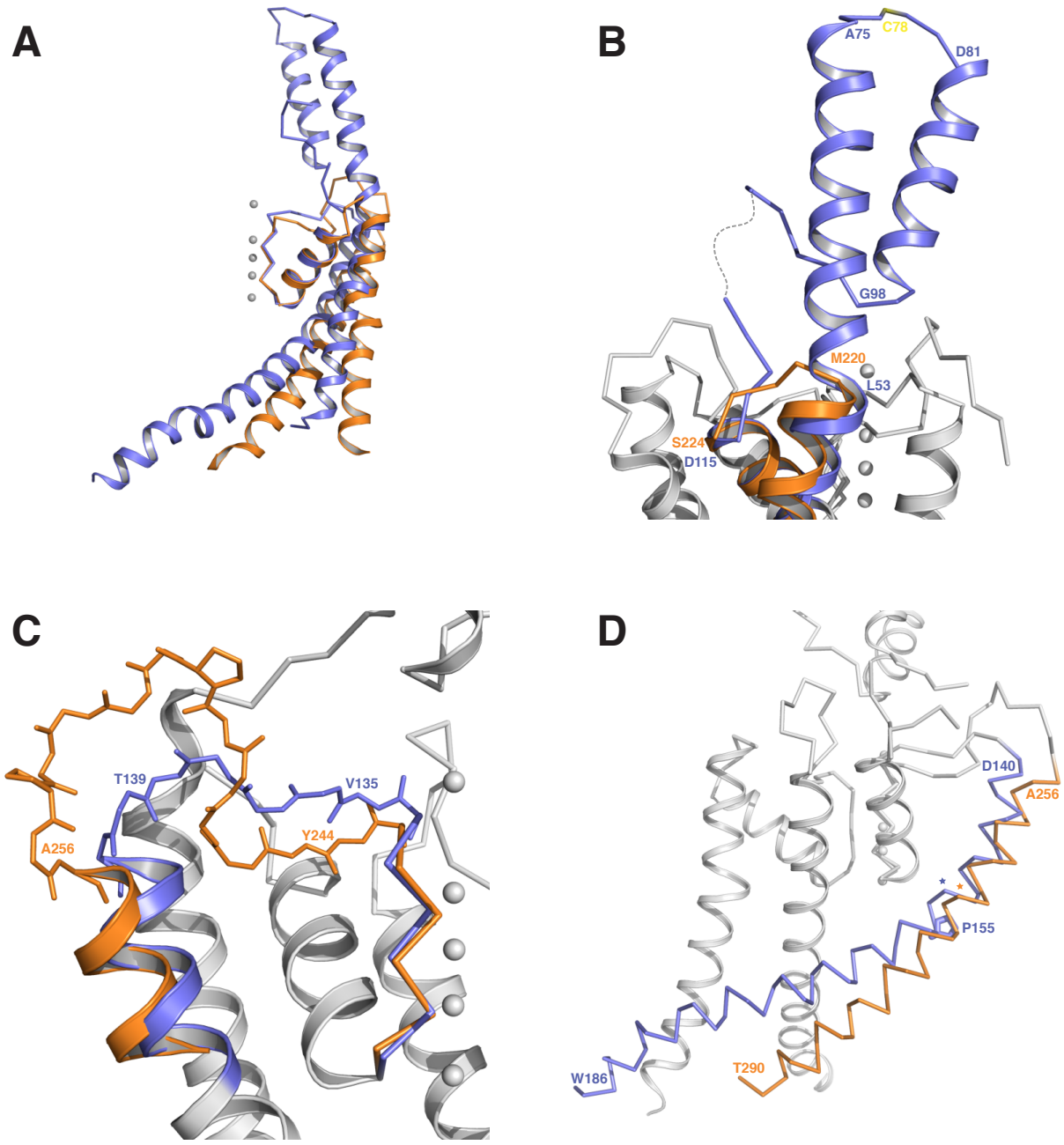
A
B
A75
C78
D81
G98
M220
L53
S224
D115
C
T139
V135
Y244
A256
D
D140
A256
P155
W186
T290

Fig. S7.

Structural asymmetry in TRAAK. (A) Overall structural differences between pore domains in TRAAK. Pore domain 2 (orange) is shown in the same view as in Fig. 1C with pore domain 1 (blue) superimposed. **(B-D)** Detailed views of structural differences between pore domain 1 and pore domain 2. **(B)** Difference between the outer helix-pore helix connections. Residues 107-111 lack interpretable electron density and are drawn as a dashed gray line. **(C)** Difference between the selectivity filter-inner helix connections. **(D)** Difference between the inner helices. Stars indicate the position of the hinge glycine in each pore domain inner helix. The first and last residue in each region and residues referred to in the text are labeled in **(B-D)**.

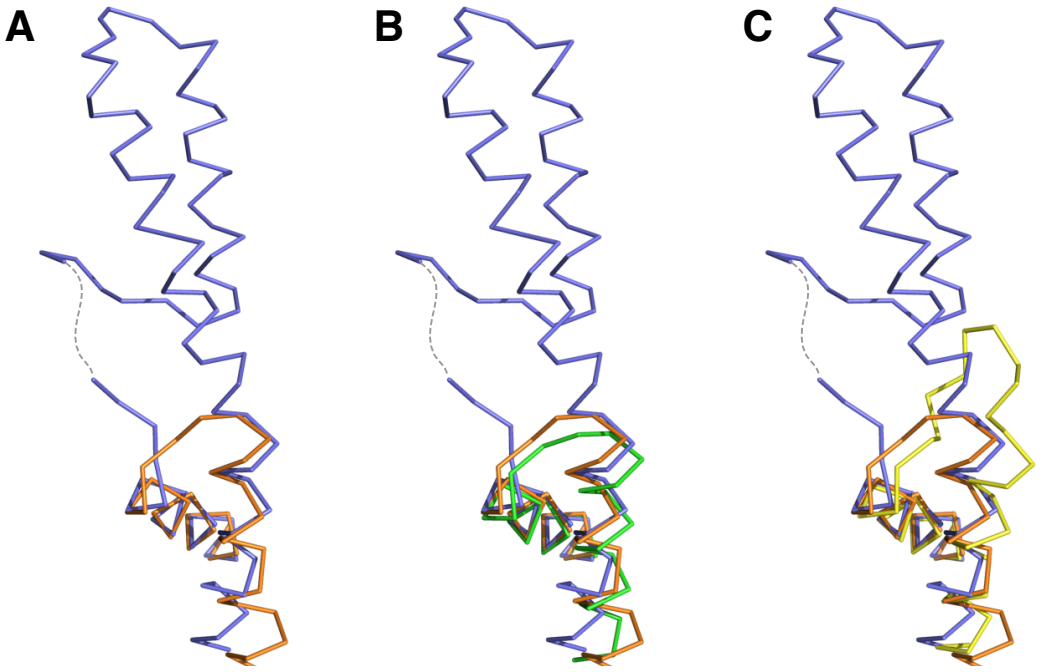
A
B
C
TRAAK pore domain 1
TRAAK pore domain 2
TRAAK pore domain 1
TRAAK pore domain 2
MthK (3LDC)
TRAAK pore domain 1
TRAAK pore domain 2
KcsA (1K4C)

Fig. S8.
Comparison of outer helix-pore helix connections in TRAAK, MthK, and KcsA.

(A,B,C) Views of the outer helix-pore helix connection similar to that in Fig. S7B. TRAAK is shown as wires with pore domain 1 blue and pore domain 2 orange in **(A)**. In **(B)**, the analogous region from MthK (green) (*25*) is superimposed. In **(C)**, the analogous region (the turret, yellow) from KcsA (*27*) is superimposed.

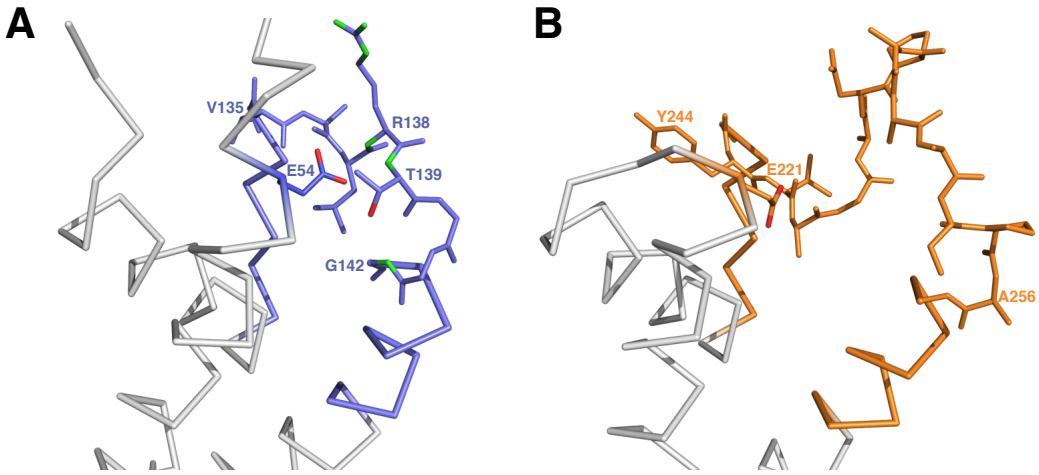
A
V135
R138
E54
T139
G142
B
Y244
E221
A256

Fig. S9.
Detailed view of the selectivity filter-outer helix connection difference between TRAAK pore domain 1 and pore domain 2. Views of pore domain 1 **(A)** and pore domain 2 **(B)** are rotated 180° with respect to (Fig. S7C). The region is shown as sticks and ribbons with pore domain 1 blue and pore domain 2 orange. Surrounding protein is shown as wire. In pore domain 1 **(A)**, oxygen atoms (red) and amides (green) forming the conserved K^+ channel outer helix-inner helix interaction network are displayed. T139 is positioned to hydrogen bond with the backbone amide of G142 at the extracellular end of the inner helix. The backbone amides of R138 and T139 are in turn positioned to interact with the side chain of the conserved E54 from the extracellular end of the outer helix. This set of interactions is conserved in all known K^+ channel structures except for the eukaryotic inward rectifiers (*28*) where a disulfide bond between cysteines in analogous positions to T139 and E54 tethers the inner helix to the channel core. In **(B)**, E221 is shown, but it does not form a similar interaction network with residues at the extracellular end of the inner helix in pore domain 2 due to the extended linker and lateral displacement of the outer helix from the channel core. E221 is in an analogous position to E54 from pore domain 1, but is not conserved in pore domain 2 of K2P channels.

A

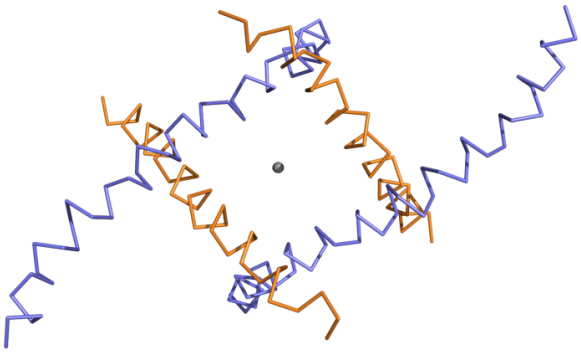

TRAAK pore domain 1
TRAAK pore domain 2

B

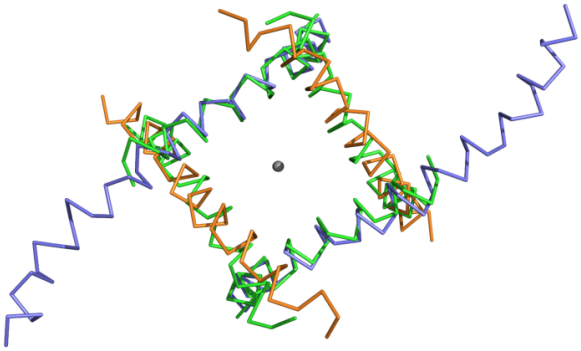

TRAAK pore domain 1
TRAAK pore domain 2
MthK (3LDC)

C

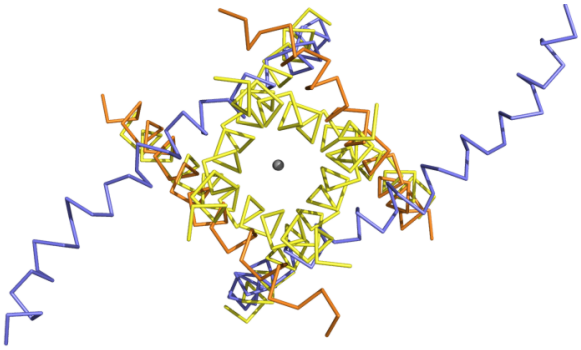

TRAAK pore domain 1
TRAAK pore domain 2
KcsA (1K4C)

D

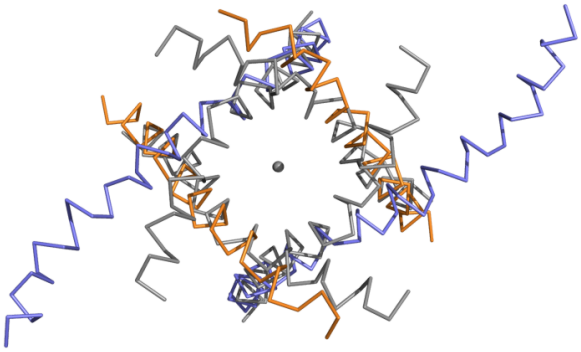

TRAAK pore domain 1
TRAAK pore domain 2
Kv1.2-2.1 (2R9R)

Fig. S10.
Comparison of the inner helix arrangement in TRAAK, MthK, KcsA, and Kv1.2-2.1. (A) Inner helices of TRAAK in wire representation viewed from the cytoplasmic side. Pore domain 1 is colored blue and pore domain 2 is colored orange with K^+ ions shown as gray spheres. In **(B)**, the inner helices from MthK (green, open conformation) (*25*) are superimposed. In **(C)**, the inner helices from KcsA (yellow, closed conformation) (*27*) are superimposed. In **(D)**, the inner helices from Kv1.2-2.1 (gray, open conformation) (*30*) are superimposed.

Table S1. Crystallographic data collection and model refinement statistics.

Data collection

Data set	Native[a]	Tl^+ peak	Tl^+ inflection	CH_3Hg^+ peak
Space group	$p2_12_12_1$	$p2_12_12_1$	$p2_12_12_1$	$p2_12_12_1$
Lattice constants (Å)	a=87.9 b=130.9 c=132.8 α=β=γ=90°	a=87.5 b=130.7 c=132.1 α=β=γ=90°	a=87.5 b=130.7 c=132.1 α=β=γ=90°	a=87.2 b=128.6 c=135.5 α=β=γ=90°
Beamline	APS 23-IDD	APS 23-IDD	APS 23-IDD	APS 23-IDB
Wavelength (Å)	0.97833	0.97833	0.97914	1.00604
Resolution (Å)	40.0 - 3.3 (3.4 - 3.3)[b]	40.0 - 4.2 (4.3 - 4.2)	40.0 - 4.2 (4.3 - 4.2)	40.0 - 5.0 (5.1 - 5.0)
Unique reflections	17761	11492	11619	6940
I/σI	25.6 (1.4)	15.6 (1.3)	14.2 (1.1)	34.0 (1.2)
Redundancy	3.7 (4.5)	3.6 (3.7)	3.6 (3.7)	7.9 (8.1)
Completeness (%)	73.4 (4.9)	98.2 (99.3)	98.4 (99.3)	99.8 (100)
R_{sym}[c]	0.056 (0.948)	0.089 (0.943)	0.067 (>1.0)	0.059 (>1.0)

Refinement

Resolution (Å)	31.2 - 3.3
Number of reflections	16792 (880)[d]
R_{work} (%)	31.7
R_{free} (%)	32.3
Protein atoms, K^+ ions	3740, 5
Mean B value[e]	167.7
Ramachandran plot (%)[f]	93.1 / 6.9 / 0
R.M.S.D. bond lengths (Å)[g]	0.008
R.M.S.D. bond angles (°)	1.172

[a] Native data were anisotropically truncated to 3.8 x 3.3 x 3.8 Å prior to scaling.
[b] Numbers in parentheses represent values for the highest resolution shell.
[c] $R_{sym} = \Sigma | I_i - \langle I_i \rangle | / \Sigma I_i$, where $\langle I_i \rangle$ is the average intensity of symmetry related reflections.
[d] Number of reflections in free set.
[e] An additional isotropic B value of -74 was applied to the scaled data.
[f] The three values represent the percentage of residues in the most favored, additionally allowed, and disallowed regions, respectively.
[g] Root mean-squared deviation from ideal values.